

Title	Carrier trapping study on a Ge nanocrystal by two-pass lift mode electrostatic force microscopy
Authors	Lin, Zhen;Brunkov, Pavel N.;Bassani, Franck;Descamps, Armel;O'Dwyer, Colm;Bremond, Georges
Publication date	2015-03
Original Citation	Lin, Z., Brunkov, P., Bassani, F., Descamps, A., O'Dwyer, C. and Bremond, G. (2015) 'Carrier trapping study on a Ge nanocrystal by two-pass lift mode electrostatic force microscopy', Materials Research Express, 2(3), 035001 (10pp). doi: 10.1088/2053-1591/2/3/035001
Type of publication	Article (peer-reviewed)
Link to publisher's version	http://iopscience.iop.org/2053-1591/2/3/035001/article - 10.1088/2053-1591/2/3/035001
Rights	This is an author-created, un-copyedited version of an article accepted for publication in Materials Research Express. The publisher is not responsible for any errors or omissions in this version of the manuscript or any version derived from it. The Version of Record is available online at https://doi.org/10.1088/2053-1591/2/3/035001
Download date	2025-04-20 04:08:24
Item downloaded from	https://hdl.handle.net/10468/6200



UCC

University College Cork, Ireland
Coláiste na hOllscoile Corcaigh

Electrostatic Force Microscopy Study on Trapped Charges in an Isolated Ge Nanocrystal for Memory Applications

Z. Lin^{1,2}(林振), P. Brunkov³, F. Bassani⁴, A.Descamps⁵, C. O'Dwyer^{6,7}, G. Bremond²

- ¹⁾ *Institut des Nanotechnologies de Lyon – INL/UMR 5270, CNRS, Ecole Centrale de Lyon, 36 avenue Guy de Collongue, 69134 Ecully Cedex, France*
- ²⁾ *Université de Lyon, Institut National des Sciences Appliquées de Lyon, Bât. Blaise Pascal, 20, avenue Albert Einstein - 69621 Villeurbanne Cedex, France*
- ³⁾ *Ioffe Physical-Technical Institute of the Russian Academy of Sciences, Saint-Petersbourg, 194021, Russia*
- ⁴⁾ *Institut Matériaux Microélectronique Nanosciences de Provence, UMR CNRS 6242, Université paul cézanne, Avenue Escadrille Normandie-Niemen - Case 142, F-13397 Marseille Cedex 20, France*
- ⁵⁾ *Centre Lyonnais de Microscopie, CLYM platform facility, 69621 Villeurbanne Cedex, France*
- ⁶⁾ *Department of Chemistry, University College Cork, Cork, Ireland, and*
- ⁷⁾ *Micro & Nanoelectronics Centre, Tyndall National Institute, Lee Maltings, Cork, Ireland*

Abstract: Trapped charges inside an isolated Germanium nanocrystal (Ge_NC) have been studied by Electrostatic Force Microscopy (EFM) two-pass lift mode measurement at room temperature. From visualized EFM images, electrons and holes were proved to be successfully injected and trapped in the Ge_NC and distributed homogenously at the edge of its truncated spherical morphology. Such Ge_NC is found to have iso-potential surface and behave as a conductive material after being charged. It is also shown that the dominant charge decay mechanism during discharging of Ge_NC is related to the leakage of these trapped charges. A truncated capacitor model is used to approximate the real capacitance between the tip and Ge_NC surface and to quantitatively study these trapped charges. These investigations demonstrate the potential for Ge nanocrystal memory applications.

Key words: Nanostructure, Germanium, Nanocrystal, Electrostatic Force Microscopy, Memory device

Nowadays, the semiconductor technology is facing a great challenge to improve device performance while reducing feature dimensions, approaching size regimes where surface effects become very important for electrical transport and biasing. This size downscaling in the microelectronics industry has initiated an explosive development of various microscopy

1
2
3 techniques to probe and reveal new physical characteristics at the nanoscale such as Coulomb
4 blockade, quantized charging effects¹⁻³ and single electron transistors⁴⁻⁵.

6
7 Due to the increasing demands for information storage and the significant scaling
8 limitations of traditional memories, the non-volatile memory device composed of Silicon (Si)
9 or Ge nanodots are very promising⁶⁻⁸. Altering the oxide thickness and voltage operation can
10 directly influence charge storage, and nanoscale crystals are promising since they have fast
11 tunnelling-mediated write times⁹⁻¹⁰. Thus, the characterisation and understanding of the
12 charging mechanism in such nanostructures is of prime importance. However, most of the
13 studies of charge trap in Ge nanocrystals were done by microscope in micro dimension.

14
15 Variations on atomic force microscopy can provide simultaneous topography and various
16 physical feature images with some additional applications such as scanning capacitance
17 microscope (SCM), electrostatic force microscope (EFM), scanning tunnelling microscope
18 (TUNA) and Kelvin probe force microscope (KPFM)¹¹⁻¹⁶. Electrostatic Force Microscopy
19 (EFM) is used specially for characterizing materials for accurate local and non-destructive
20 electrical properties for a wide range of characterisations such as surface potential, charge
21 distributions and dielectric constant¹⁷. EFM is also able to easily and non-destructively inject
22 and detect the localised charge in nanostructures, on or below the surface by a special two-
23 pass lift mode. This ability has been used to study the distribution of trapped charges in
24 silicon dioxide layer or implanted nano crystals¹⁸⁻²¹. However, the characterisation of isolated
25 Ge_NC was few studied by EFM at room temperature. Such nanostructures are of a great
26 interest because the injected carriers are strongly constrained in their propagation, and interact
27 with a finite geometry which should be generally the case in nano-electronic devices.

28
29 In this study, isolated Ge_NC on a silicon dioxide layer on n⁺ type doped silicon (001)
30 substrate has been shown to exhibit charge storage memory effects by EFM two-pass lift
31 mode measurement at room temperature. The accurate phase signal conducted by electrostatic
32 force interactions was used to determine the charge retention time inside the Ge_NCs. The
33 charge storage and retention effects are discussed in the context of Ge NC memory
34 application. In order to quantitatively study these trapped charges, a truncated capacitor model
35 was used to approximate the real capacitance between the tip and island surface. The quantity
36 of charged electrons was calculated by analytical expression of the charge quantity in function
37 of the EFM phase signal.

38
39 These nano-scale Ge_NCs have been fabricated on top of a very thin silicon dioxide layer
40 using a dewetting processing. A 15 nm thick Ge layer was deposited by molecular beam
41 epitaxy (MBE) over the SiO₂ layer 5 nm in thickness at ambient temperature and was

thermally annealed at 750°C for 20 minutes under ultrahigh vacuum. This process leads to the formation of crystalline Ge NCs having an average diameter ~150 nm. As it has been shown in previous work²², the Ge_NC diameter is ~7 times the nominal thickness of the Ge layer. Over the dots there is a natural oxide layer of ~2 nm so that the sample surface is uneven, comprising a dispersion of Ge NCs.

FIG.1 Sample structure with Ge_NC's on SiO₂ layer

In order to minimize the influence of morphology over the sample surface during charge measurement, Electrostatic Force Microscopy (EFM) was chosen for charging experiment. EFM measurements are acquired in a two-pass lift mode. In this measurement, a constant separation between the tip and local surface topography²² when the tip rises to the lift scan height and this maintains a constant van der Waal's interactions. This allows the imaging of relatively weak but long range electrostatic interactions while minimizing the influence of topography.

Modelled by simple parallel plate capacitor, the electrostatic force between a conductive tip and a sample surface can be described as:

$$F = \frac{1}{2} \frac{\partial C}{\partial z} (\Delta V)^2 = \frac{1}{2} \frac{\partial C}{\partial z} (V_t - V_s)^2 \quad (1)$$

where C is the effective capacitance between the EFM probe and the sample; V_t and V_s are the tip and sample bias, respectively. If the sample surface has a certain area that has locally trapped electric charges, V_s will become the surface potential V_q , which is modified by these trapped charges and causes changes in the electrostatic force intensity and the effective spring constant of the cantilever²².

The resonant frequency, ω of vibration of the cantilever varies as

$$\omega = \omega_0 \sqrt{1 - \frac{1}{k} \frac{dF}{dz}} \quad (2)$$

where $\partial F/\partial z$ is the electrostatic force gradient acting on the EFM probe by these charges. The frequency changes due to the local electrostatic forces could easily be monitored by observing the phase shift of the resulting cantilever vibration.

The phase shift can be expressed as follows:

$$\Delta\phi = -\frac{Q}{k} \frac{\partial F}{\partial z} (z_0) = -\frac{Q}{2k} \frac{d^2 C}{dz^2} (V_{EFM} - V_q)^2 \quad (3)$$

where Q is the quality factor of AFM probe, k is the spring constant of the cantilever (2.8 N/m), z is the height between the tip and the sample surface, V_{EFM} and V_q are, respectively, the tip and sample surface potential during charge measurement.

The EFM measurement was conducted on a Veeco Digital Instruments 3100 Dimensions AFM employing a Nanoscope V controller. Charges were injected by using commercial conductive SCM-PIT tip. Its main specifications are: cantilever spring constant, and $\omega_0 = 75$ kHz. Specifically, the tip is coated with a Pt/Ir metal coating.

From (3), a sign change and alteration of V_{EFM} can induce a bump or a depression in $\Delta\phi$. Firstly, a p-type silicon (001) substrate with a 3 nm native oxide layer was charged separately by -7 V in Fig. 2(a) and +7 V in Fig. 2(b) over 30s. The V_{EFM} was set separately at +2 V (top region) and -2 V (bottom region below). The charged area response is shown in the phase signal. Different signs of V_{EFM} can change the image colour in the charged region from black to white, which corresponds to a depression or a peak from the phase profiles. By flipping the polarity of the applied voltage the reverse response is found. The uneven surface in the phase image is caused by injected charges that change the sample surface potential.

FIG.2 A 3 nm SiO₂ over a p-type Si (001) substrate charged by: (a) -7 V for 30 s, tip bias = +2V in top region above and -2V in the bottom region; (b) +7 V for 30 s, tip bias = +2V for the top region and -2V in the bottom region.

The original surface phase signal for charge-based memory effects was also measured before charge injection into a sample of Ge_NCs on oxidized Si, using two polarities of tip bias (V_{EFM}) of with a magnitude of ± 2 V, and height of 50 nm. The resulting phase image is shown in Fig. 3(b). The average diameter of the Ge_NCs is 150 nm. The phase signal is found to be higher in the centre of the NC than at the periphery, indicated by its corresponding peak in the phase signal. Additionally, the phase value in (c) was larger than that in (b). Considering the only change is the polarity and magnitude of V_{EFM} during these two measurements, it confirms that the Ge_NC has quite a weak original positive surface potential V_q .

FIG.3 Ge NCs with an average diameter of 150 nm prior to charging, (a) Topography, (b) Phase signal images of Ge NCs acquired at $V_{EFM} = +2V$, (c) Phase signal images acquired at $V_{EFM} = -2V$.

To demonstrate the memory effect based on charging and discharging of individual Ge NCs, an individual Ge NC was identified for charging. For the charging process, the conductive tip was kept at the same position over the isolated NC and subsequently brought closer to the NC

1
2
3 surface. At the same time, charges were injected by polarising the tip with a voltage stress of
4 either +7 V or -7 V for 30 seconds. The corresponding EFM phase images are shown in Fig. 4,
5 where the charged region of the NCs is marked.
6
7

8
9
10 FIG.4 EFM images after charging at +7 V / -7V for 30s. Holes and Electrons were separately injected into the isolated Ge NC
11 as marked. Phase signal images acquired at $V_{EFM} =$ (a) +2 V, (b) -2 V, (c) 0V, the scan size is $1 \mu\text{m} \times 1 \mu\text{m}$, and (d) +2V, the
12 scan size is $3 \mu\text{m} \times 3 \mu\text{m}$.
13
14

15 From the EFM measurements on single NC, the charged area can be readily identified.
16 During the charging process, holes (+7 V, extracted) or electrons (-7 V, injected) are injected
17 the isolated Ge_NC where they can form an electron cloud from the phase images. To
18 maximize the resolution of the phase signal a V_{EFM} with the opposite polarity to V_q is used.
19 The phase shift inside the charged NC is detected at 0.5° ($V_{EFM} = +2$ V) and 1° ($V_{EFM} = -2$ V)
20 for +7 V whereas its value is -4.5° ($V_{EFM} = +2$ V) and -2.5° ($V_{EFM} = -2$ V) at the opposite bias
21 of -7 V. This suggests that it is much easier to inject electrons than holes into Ge NCs.
22
23

24 A particular phenomenon found for charge transfer into Ge NCs is charge localization that
25 is influenced by morphology. From Fig. 4, the injected charges can be trapped homogenously
26 by the isolated NC and located in the corner of edge. Such Ge NC became iso-potential and
27 behaved as a conductive material after being charged. It is confirmed that these charges were
28 successfully injected into the isolated Ge_NC.
29
30

31 Additionally, from (3), the value of V_{EFM} can greatly influence the phase shift $\Delta\phi$.
32 Therefore, comparison between an uncharged and a charged area or these areas charged by
33 different voltages for a fixed V_{EFM} (tip surface potential) is necessary.
34
35

36 The discharge and retention time of these trapped charges were also evaluated. From Fig.
37 5(a), the EFM phase signal is plotted versus time after charging. The phase amplitude in the
38 charged region decreases gradually due to charge dissipation. It is shown that the dominant
39 charge decay mechanism during discharging is the leakage of these trapped charges. The Ge
40 NC is p-type and forms a p-n junction with n-Si, with the associated potential barrier allowing
41 charger to be stored without immediate (Ohmic) discharge/conduction.
42
43

44
45
46
47
48
49
50
51
52
53
54
55 FIG.5 (a) Discharge procedure of trapped charges in the centre of NC, (b) Altitude of charged area (c) Phase signal in the
56 centre of charged area
57
58

59 Fig. 5(b), (c) shows the EFM phase image with different tip bias voltage V_{EFM} (from -5 V
60 to +4 V). The phase intensity of the charged NC follows the magnitude of the tip bias ($|V_{EFM}|$),

where in Fig. 5(b), this corresponds to the strength of electrostatic force between tip and charged NC. In Fig. 5 (c), phase signal in the centre of the charged region increases with tip bias, and specifically, a negative tip bias alters the indicative phase signal more than a positive bias. This observation confirms that the setup of a p-n junction barrier allows trapped charges to be stored with a certain retention time. This is consistent with the experimental evidence that using opposite tip biases for V_{EFM} and V_q markedly improves resolution in EFM phase image (by at least a factor of 4).

In order to quantitatively characterize the trapped charges, equivalent structures should be used for modelling the interaction between AFM tip and sample surface. The electrostatic force between a conductive tip and a sample surface could be described as²⁰:

$$F_s = \frac{1}{2} \frac{\partial C}{\partial z} (\Delta V)^2 = \frac{1}{2} \frac{\partial C}{\partial z} (V_t - V_s)^2 \quad (1)$$

Where C is the effective capacitance between the EFM probe and the sample, V_t and V_s are, respectively, the tip and sample potential. If the sample surface has a certain area that has locally trapped electric charges, V_s will become the surface potential V_q which is modified by these trapped charges and causes changes in the electrostatic force intensity and its gradient. The force gradient changes the effective spring constant of the sensor and, consequently, its resonance frequency ω_r .

$$\omega_r \approx \omega_0 \left(1 - \frac{1}{2k} \frac{\partial F}{\partial z} (z_0) \right) \quad (2)$$

These changes could easily be detected by the phase shift $\Delta\phi$.

$$\Delta\phi = -\frac{Q}{k} \frac{\partial F_s}{\partial z} (z_0) = -\frac{Q}{2k} \frac{d^2 C}{dz^2} (V_{EFM} - V_q)^2 \quad (3)$$

Where Q is the quality factor of AFM probe, k is the spring constant of the cantilever, z is the height of the tip with respect to the surface, $\partial F_s / \partial z$ is the spatial derivative of the electrostatic force acting on the EFM probe by these charges, V_{EFM} is the tip potential during the EFM measurement.

The AFM probe is composed of three main parts: the cantilever, the tip and the tip apex. During the AFM measurement, these three parts interact with the sample surface and can be modelled simply as a series of flat plane capacitances. The cantilever is modelled as a flat plane, the tip is modelled as a truncated cone²¹ and the tip apex is modelled as a small sphere or the tip and its apex as a cone. From the theoretical studies, it shows that the major contribution to the capacitance variation is given by tip apex, followed far below by the cone,

chip and cantilever²². So the truncated cone-plane model is relatively the most accurate one which considers the tip apex and the tip body.

Plane-plane capacitance model:

$$\frac{\partial^2 C}{\partial z^2} = C''(z) = 2\epsilon_0\epsilon_r \frac{S}{z^3} \quad (4)$$

Truncated cone-plane model (total tip apex and tip body) gives the second derivative capacitance factor $C''_{tcp}(z)$:

$$C''_{tcp}(z) \approx 2\pi\epsilon_0 \left[\frac{R^2(2z+R)}{z^2(z+R)^2} + k^2 \left(\frac{1}{z+R} + \frac{R}{\sin\theta(z+R)^2} \right) \right] \quad (5)$$

with $k = \frac{1}{\ln\left(\cot\left(\frac{\theta}{2}\right)\right)}$

Where R is the tip apex radius and θ is the tip-opening angle.

The equivalent electric circuit of this experiment configuration is given in Fig.6.

FIG.6. Equivalent circuit

Where C_1 is the charged island-substrate capacitance, C_2 is the charged island-tip capacitance and C_3 is the substrate-probe capacitance.

Thus, electrostatic force due to these trapped charges could be expressed as:

$$F = \frac{1}{2} \left(\frac{C_1 V - q}{C_1 + C_2} \right)^2 \frac{dC_2}{dz} + \frac{1}{2} V^2 \frac{dC_3}{dz} \quad (6)$$

For SCM-PIT, the tip height is 10~15um and R is 20nm with a tip-opening angle of 10°. The lift height is always set at 50nm. The variation of the second derivative capacitance $C''(z)$ which varies with the tip-surface distance z is plotted in Fig.7. We can observe that the effective surface during the tip scan is about $7.1 \times 10^3 \text{ nm}^2$ considering the realistic tip-surface model and a lift height of 50 nm. This effective surface corresponds to a disc area with 95 nm in diameter which is lower than that of the Ge_NC.

FIG.7. Second derivative capacitance versus tip surface distance

The diameter of these isolated Ge_NC is more than 100 nm. However, the SCM-PIT tip has a radius from 20 to 25 nm which is quite smaller than the island surface and the effective area is inside it. So these truncated-sphere shape islands could be simplified as rectangular nano

structures which has a flat surface interacting with the tip, see Fig.8. This simple model could be used for quantifying trapped charges in oxide layers or embedded conductive nanostructures^{23, 24}.

FIG.8. Simplified nano-scale Ge_NC model

Using the parallel plate capacitor model, the total charge q inside the trapped area can be deduced as below:

$$q = \frac{\Delta\phi \times k \left(z_0 + \frac{d_{SiO_2}}{\epsilon_{SiO_2}} + \frac{d_{Ge}}{\epsilon_{Ge}} \right)^3 \epsilon_0 S}{Q \left(\frac{d_{SiO_2}}{\epsilon_{SiO_2}} + \frac{d_{Ge}}{\epsilon_{Ge}} \right)^2} \quad (7)$$

$$D = \frac{q}{S} \quad (8)$$

Where k is the cantilever spring constant, Q is the quality factor of the AFM probe and S is the effective tip area. D is the the charge density in this charged area.

In our experiment, k is 1~5 N/m, Q is about 250, the dielectric constants for SiO_2 and Ge are 3.9 and 16.2 respectively, the charged Ge dot height is about 100 nm and S is $7.1 \times 10^3 \text{ nm}^2$. Therefore, when the isolated Ge_NC is charged by -7V during 30 seconds (EFM phase image in Fig.4(a) and (c), electron injection), the injected charges density in the centre of the island is about $7.2 \times 10^{-18} \text{ C}$ and that at the edge is about $1.1 \times 10^{-17} \text{ C}$. The charge density along the detecting line can be drawn in Fig.9.

FIG.9. (a) phase image after charge (b) charge density along trapped line

From Fig.9, the value of charge density was higher at the edge than that inside the charged island. This means that the Ge_NC became iso-potential and behaved as a conductive material that caused these trapped charges locating in the corner of its sphere surface.

In the whole charge area, according to our calculation, there are in an amount of 800 electrons injected to this isolated nano-scale Ge_NC.

In summary, EFM two-pass lift mode measurement at room temperature confirmed trapped charges could be stored on single Ge_NC on oxidized silicon. Electrons and holes were successfully injected into the Ge_NC by a conductive EFM tip. Optimised EFM bias settings for better EFM charge signals have been determined. In order to achieve higher resolution in

1
2
3 phase imaging, V_{EFM} with opposite polarity to V_q is preferred. Such Ge_NC's have iso-
4 potential values and behave as a conductive material once charged. The injected charges are
5 also demonstrated to be trapped homogeneously by the isolated NC. Trapped electrons inside a
6 100 nm NC discharged gradually over 2 hours. By varying the magnitude of the tip scan bias,
7 an improvement in the phase signal can be achieved with the use of a negative tip bias,
8 keeping the sample bias positive for this system. By applying a tip bias of -7V during 30
9 seconds leads to an injection of about 800 electrons inside an individual Ge_NC. This study is
10 of prime importance in developing electronic devices such as memory transistors using
11 Ge_NC.
12
13
14
15
16
17
18
19
20
21
22
23

24 REFERENCES

- 25
- 26 1. J. W. G. Wildöer, L. C. Venema, A. G. Rinzler, R. E. Smalley, C. Dekker, *Nature* 59,
- 27 391, (1998).
- 28 2. T. W. Odom, J.L. Huang, P. Kim, C. M. Lieber, *Nature* 62, 391, (1998).
- 29 3. S. J. Tans, R. M. Verschueren, C. Dekker, *Nature* 49, 393, (1998).
- 30 4. M. T. Woodside and P. L. McEuen, *Science* 296, 1098, (2002).
- 31 5. J.W. Park, A. N. Pasupathy, J. I. Goldsmith, C. Chang, Y. Yaish, J. R. Petta, M.
- 32 Rinkoski, J. P. Sethna, H. D. Abruña, P. L. McEuen, and D. C. Ralph, *Nature* 417, 722
- 33 (2002)
- 34 6. W. H. Chen, C. H. Liu, Q. L. Li, Q. J. Sun, J. Liu, X. Gao, X. H. Sun and S. D. Wang,
- 35 *Nanotechnology* 25, 075201, (2014).
- 36 7. O. Graydon, *Nature Photonics* 7, 2, (2013).
- 37 8. M. Yang, T.P. Chen, J.I. Wong, Y. Liu, A.A.Tseng, S. Fung, *Journal of nanoscience*
- 38 *and nanotechnology* 10(7), 4517, (2010).
- 39 9. Michele Sessolo, Henk J. Bolink, Hicham Brine, Helena Prima-Garcia, Ramon Tena-
- 40 Zaera, *Journal of Materials Chemistry* , 22, 4916 (2012).
- 41 10. Lun-Chun Chen, Yung-Chun Wu, Tien-Chun Lin, Jyun-Yang Huang, Min-Feng Hung,
- 42 Jiang-Hung Chen, and Chun-Yen Chang, *IEEE ELECTRON DEVICE LETTERS*, 31,
- 43 12 (2010).
- 44 11. G. Binnig, C. Gerber and C. F. Quate, *Phys. Rev. Lett.* 56, 930 (1989).
- 45 12. Z. Lin, G. Bremond and F. Bassani, *Nanoscale Research Lett.* 6, 163, (2011).
- 46 13. Z. Lin, P. Brunkov, G. Bremond, F. Bassani, *Appl. Phys. Lett.* 97, 263112 (2010).
- 47 14. S. G. Lemay, J. W. Janssen, M. van den Hout, M. Mooij, M. J. Bronikowski, P. A.
- 48 Willis, R. E. Smalley, L. P. Kouwenhoven, C. Dekker, *Nature* 412, 617, (2001).
- 49 15. T. W. Odom, J.-L. Huang, C. L. Cheung, C. M. Lieber, *Science* 290, 1549, (2000).
- 50 16. V. Madhavan, W. Chen, T. Jamneala, M. F. Crommie, N. S. Wingreen, *Science* 280,
- 51 567, (1998).
- 52 17. T. Me´lin, D. Deresmes, D. Stie´venard, *Appl. Phys. Lett.* 81, 5054, (2002).
- 53 18. M.J. Gordon, T. Baron, *Phys. Rev. B* 72, 165420 (2005).
- 54 19. F. Marchi, R. Dianoux, H.J.H. Smilde, P. Murd, F. Comin, J. Chevrier, J.
- 55 Electrostatics, 66, 538, (2008).
- 56
- 57
- 58
- 59
- 60

- 1
 - 2
 - 3
 - 4
 - 5
 - 6
 - 7
 - 8
 - 9
 - 10
 - 11
 - 12
 - 13
 - 14
 - 15
 - 16
 - 17
 - 18
 - 19
 - 20
 - 21
 - 22
 - 23
 - 24
 - 25
 - 26
 - 27
 - 28
 - 29
 - 30
 - 31
 - 32
 - 33
 - 34
 - 35
 - 36
 - 37
 - 38
 - 39
 - 40
 - 41
 - 42
 - 43
 - 44
 - 45
 - 46
 - 47
 - 48
 - 49
 - 50
 - 51
 - 52
 - 53
 - 54
 - 55
 - 56
 - 57
 - 58
 - 59
 - 60
20. P. D. Szkutnik, A. Karmous, F. Bassani, A. Ronda, I. Berbezier, K. Gacem, A. El Hdiy, M. Troyon, E. Phys. J. Appl. Phys., 41, 2, 103, (2008).
21. Dimension V Scanning Probe Microscope Manual from Veeco Company, 279, (2007).
22. S. Sarid, Scanning Force Microscopy, Oxford University Press, New York, (1994).
23. S.Hudlet, M.Saint Jean, C.Guthmann, J.Berger, Eur. Phys. J.B **2**, 5 (1998)
24. F. Marchi, R. Dianoux, H.J.H. Smilde, P. Murd, F. Comin, J. Chevrier, J.Electrostatics **66**, 538 (2008).
25. D.Schaadt, E.T.Yu, S.Sanar, A.E.Berkowitz, Appl.Phys.Lett. **74**, 472 (1999)
26. C.Y. Ng, T.P. Chen, H.W. Lau, Y. Liu, M.S. Tse, O.K. Tan, V.S.W. Lim, Appl. Phys. Lett. **85**, 2941 (2004).

1
2
3
4
5
6
7
8
9
10
11
12
13
14
15
16
17
18
19
20
21
22
23
24
25
26
27
28
29
30
31
32
33
34
35
36
37
38
39
40
41
42
43
44
45
46
47
48
49
50
51
52
53
54
55
56
57
58
59
60

Figures:

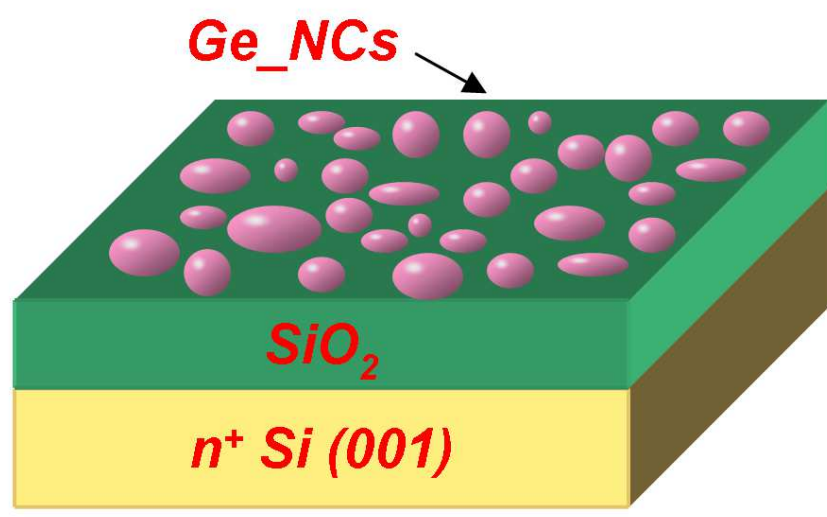


FIG.1 Sample structure with Ge_NCs on SiO_2 layer

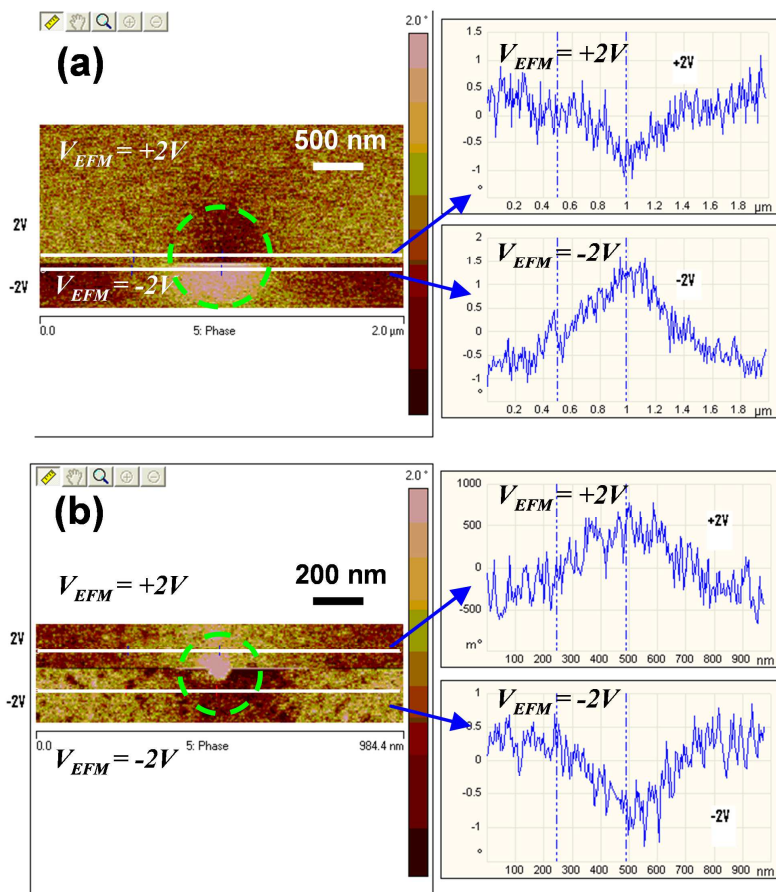


FIG.2 A 3 nm SiO_2 over a p-type Si (001) substrate charged by: (a) -7 V for 30 s, tip bias = +2V in top region above and -2V in the bottom region; (b) +7 V for 30 s, tip bias = +2V for the top region and -2V in the bottom region.

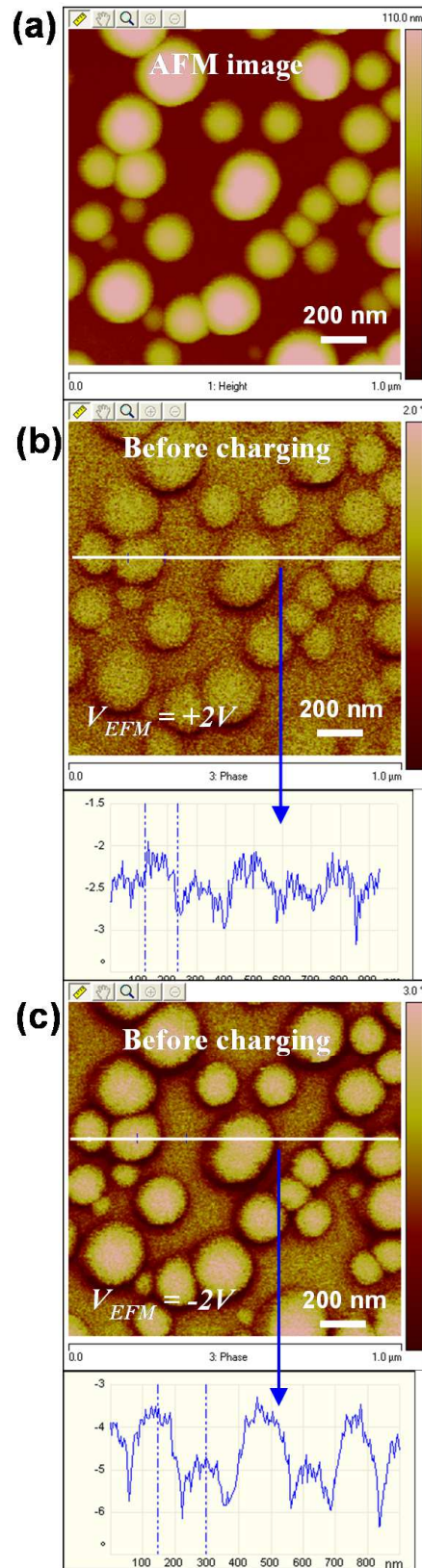


FIG.3 Ge NCs with an average diameter of 150 nm prior to charging, (a) Topography, (b) Phase signal images of Ge NCs acquired at $V_{EFM} = +2V$, (c) Phase signal images acquired at $V_{EFM} = -2V$.

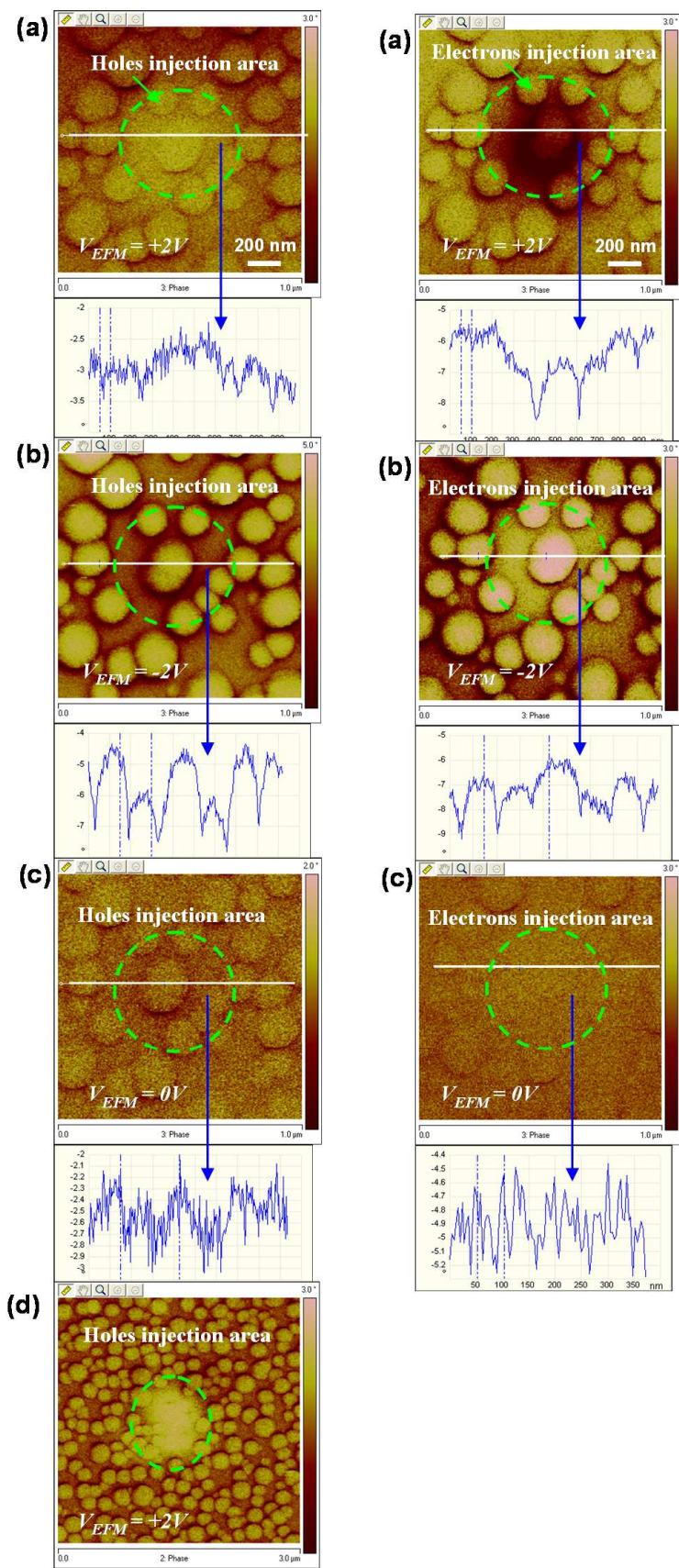


FIG.4 EFM images after charging at +7 V / -7V for 30s. Holes and Electrons were separately injected into the isolated Ge NC as marked. Phase signal images acquired at $V_{EFM} =$ (a) +2 V, (b) -2 V, (c) 0V, the scan size is $1 \mu m \times 1 \mu m$, and (d) +2V, the scan size is $3 \mu m \times 3 \mu m$.

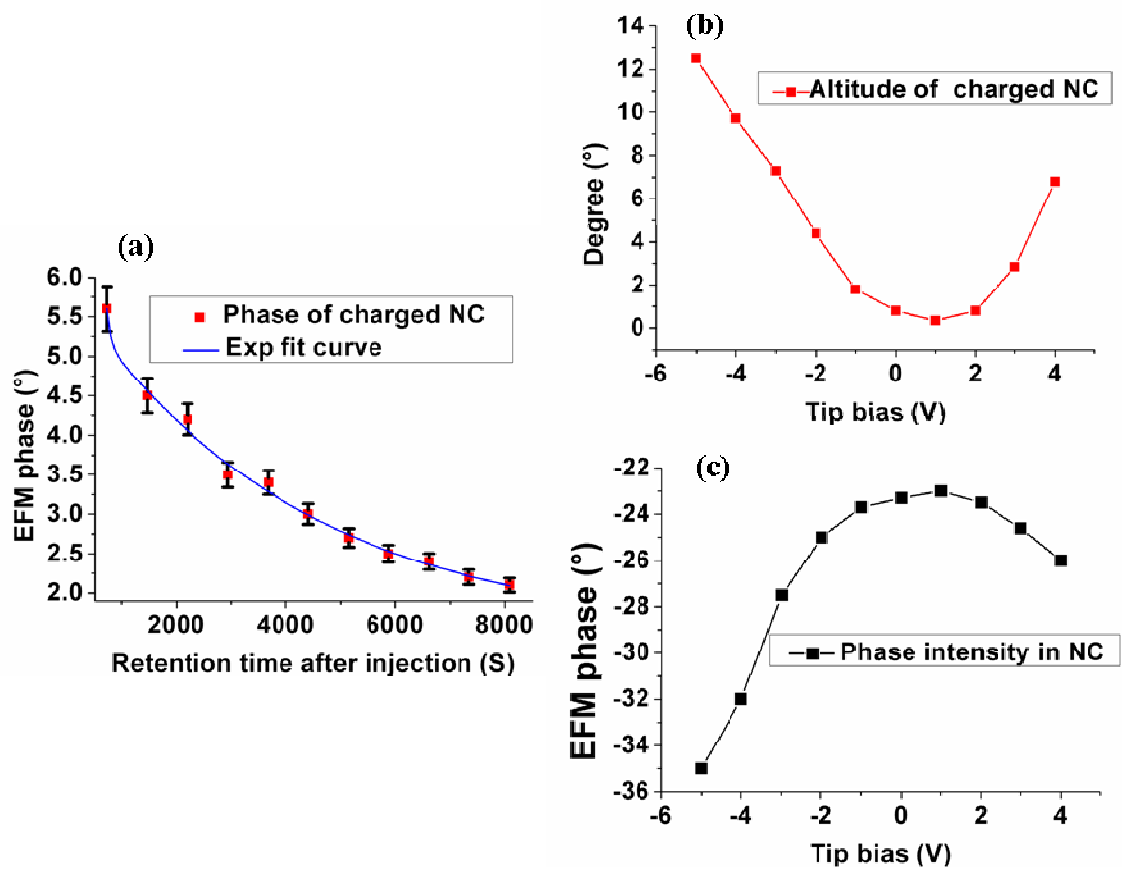


FIG.5 (a) Discharge procedure and retention time of trapped charges in the centre of NC, (b) Altitude of charged area (c) Phase signal in the centre of charged area

1
2
3
4
5
6
7
8
9
10
11
12
13
14
15
16
17
18
19
20
21
22
23
24
25
26
27
28
29
30
31
32
33
34
35
36
37
38
39
40
41
42
43
44
45
46
47
48
49
50
51
52
53
54
55
56
57
58
59
60

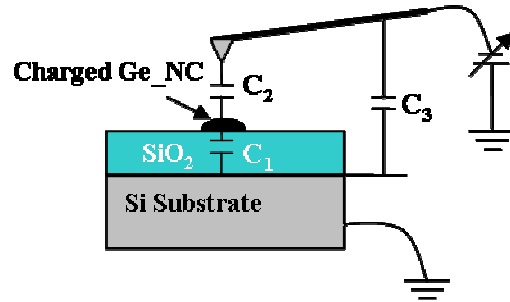


FIG.6. Equivalent circuit

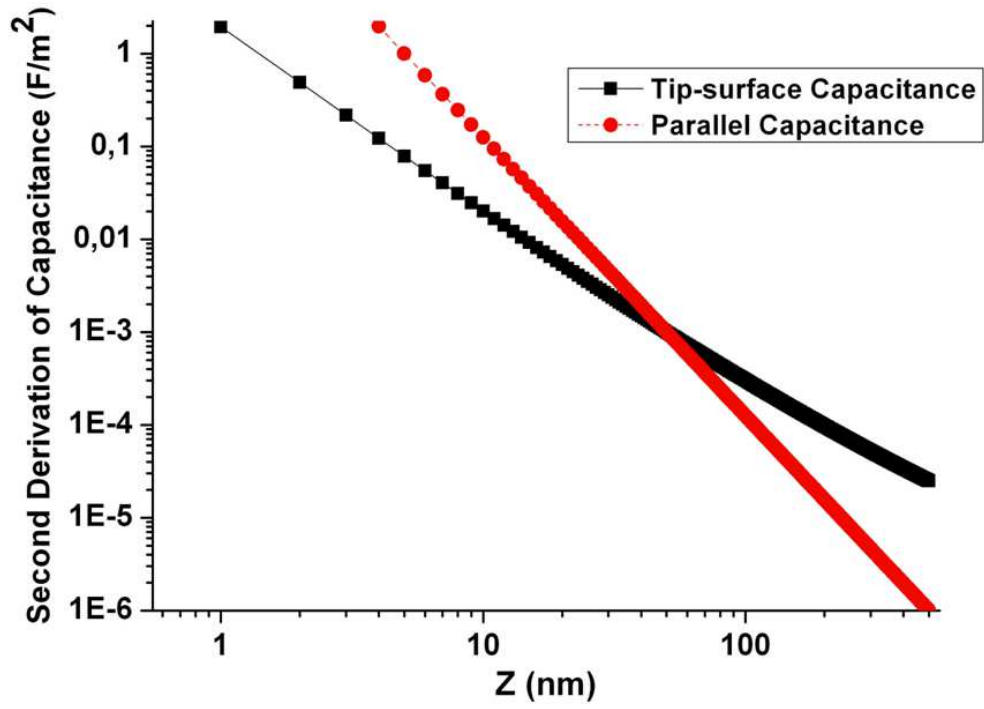


FIG.7. Second derivative capacitance versus tip surface distance

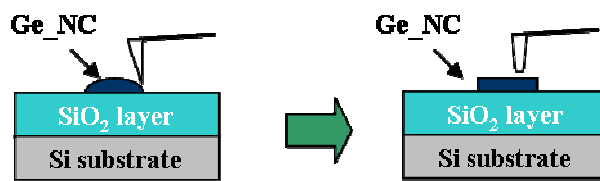


FIG.8. Simplified nano-scale Ge_NC model

1
2
3
4
5
6
7
8
9
10
11
12
13
14
15
16
17
18
19
20
21
22
23
24
25
26
27
28
29
30
31
32
33
34
35
36
37
38
39
40
41
42
43
44
45
46
47
48
49
50
51
52
53
54
55
56
57
58
59
60

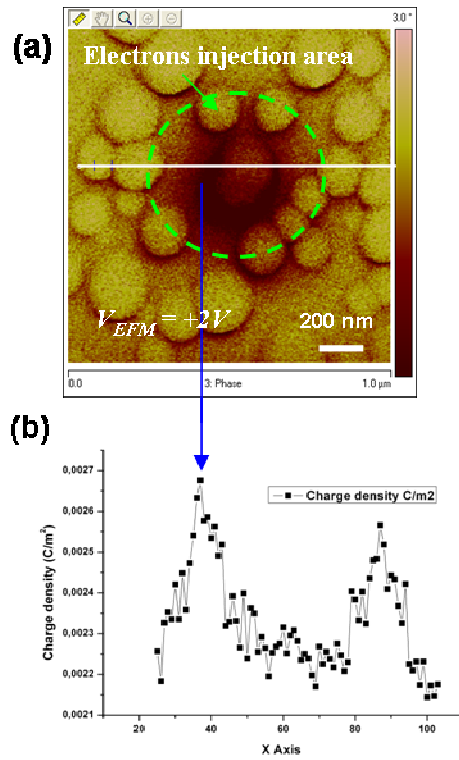


FIG.9. (a) phase image after charge (b) charge density along trapped line